ELSEVIER

Contents lists available at ScienceDirect

Acta Materialia

journal homepage: www.elsevier.com/locate/actamat



Full length article

Stationary dislocation motion at stresses significantly below the Peierls stress: Example of shuffle screw and 60° dislocations in silicon



Hao Chen^a, Valery I. Levitas b,c,d,*, Liming Xiong^e, Xiancheng Zhang^a

- ^a Key Laboratory of Pressure Systems and Safety, Ministry of Education, School of Mechanical and Power Engineering, East China University of Science and Technology, Shanghai 200237, China
- ^b Department of Aerospace Engineering, Iowa State University, Ames, Iowa 50011, USA
- ^c Department of Mechanical Engineering, Iowa State University, Ames, Iowa 50011, USA
- ^d Ames Laboratory, U.S. Department of Energy, Iowa State University, Ames, Iowa 50011-3020, USA
- e Department of Aerospace Engineering, Iowa State University, Ames, Iowa 50011, USA

ARTICLE INFO

Article history: Received 5 September 2020 Revised 19 December 2020 Accepted 31 December 2020 Available online 6 January 2021

Keywords: Dynamic Peierls stress Dislocation mobility Molecular dynamics Multiscale modeling

ABSTRACT

The stationary motion of shuffle screw and 60° dislocations in silicon when the applied shear, τ_{ap} , is much below the static Peierls stress, $\tau_p^{\rm max}$, is proved and quantified through a series of molecular dynamics (MD) simulations at 1 K and 300 K, and also by solving the continuum-level equation of motion, which uses the atomistic information as inputs. The concept of a dynamic Peierls stress, τ_p^d , below which a stationary dislocation motion can never be possible, is built upon a firm atomistic foundation. In MD simulations at 1 K, the dynamic Peierls stress is found to be $0.33\,GPa$ for a shuffle screw dislocation and $0.21\,GPa$ for a shuffle 60° dislocation, versus $\tau_p^{\rm max}$ of $1.71\,GPa$ and $1.46\,GPa$, respectively. The critical initial velocity $v_0^c(\tau_{ap})$ above which a dislocation can maintain a stationary motion at $\tau_p^d < \tau_{ap} < \tau_p^{\rm max}$ is found. The velocity dependence of the dissipation stress associated with the dislocation motion is then characterized and informed into the equation of motion of dislocation at the continuum level. A stationary dislocation motion below $\tau_p^{\rm max}$ is attributed to: (i) the periodic lattice resistance smaller than $\tau_p^{\rm max}$ almost everywhere; and (ii) the change of a dislocation's kinetic energy, which acts in a way equivalent to reducing $\tau_p^{\rm max}$. The results obtained here open up the possibilities of a dynamic intensification of plastic flow and defects accumulations, and consequently, the strain-induced phase transformations. Similar approaches can be applicable to partial dislocations, twin and phase interfaces.

© 2021 Acta Materialia Inc. Published by Elsevier Ltd. All rights reserved.

1. Introduction

As the intrinsic lattice resistance to a dislocation motion, the Peierls stress is the minimum stress required to start the motion of a static straight dislocation at zero temperature [1]. This is a key controlling parameter in many mesoscale models such as crystal plasticity [2] and dislocation dynamics [3–5]. Extensive research has been devoted to determining the Peierls stress for different materials using first principle calculations [6–11], molecular dynamics (MD) [12–18], as well as the Peierls-Nabarro model [19–21,21–24]. In different constitutive equations, it is often assumed that below the Peierls stress dislocation motion is impossible [2–5,13,25]. Here we found that the Peierls stress should be exceeded for starting the motion of a dislocation, but not to maintain its stationary motion. This concept can be understood through an anal-

E-mail addresses: vlevitas@iastate.edu (V.I. Levitas), xczhang@ecust.edu.cn (X. Zhang).

ysis of the equation of motion of dislocations at the continuum level. The energy balance equation for describing the motion of a dislocation [26] reads as

$$\tau_{ap}b\nu = \frac{dW_p(s,\tau_{ap})}{dt} + \frac{dK}{dt} + F(\nu)\nu; \quad K = 0.5m\nu^2, \tag{1}$$

where au_{ap} is the applied shear stress acting on the dislocation within the slip plane along the slip direction, b is the magnitude of the Burgers vector, v = ds/dt is the dislocation velocity, $W_p(s, \tau_{ap})$ and $\tau_p = \frac{1}{b} \frac{dW_p(s, \tau_{ap})}{ds}$ are the Peierls energy per unit length and the lattice resistance stress, respectively, which are periodic along the dislocation path s and dependent on the applied stress τ_{ap} , K and m are the kinetic energy and effective mass of a dislocation per unit length, F(v) is the dissipation force per unit length induced by the electron/phonon drag and the wave radiation from a fast moving dislocation. For $\tau_{ap} = const$, with $\frac{dW_p(s, \tau_{ap})}{dt} = \frac{dW_p(s, \tau_{ap})}{ds} \frac{ds}{dt} = \frac{dW_p(s, \tau_{ap})}{ds} v = \tau_p bv$, and $\frac{dK}{dt} = mv \frac{dv}{dt}$, Eq. (1) can be re-written as

$$\tau_{ap}b = \tau_p b + m \frac{dv}{dt} + F(v). \tag{2}$$

^{*} Corresponding author.

It is clear from Eq. (2) that, at a zero initial velocity, $\nu_0=0$, a dislocation does not move until $\tau_{ap}>\tau_p^{\rm max}$. That is why the Peierls stress $\tau_p^{\rm max}$ is considered as a counterpart of the dry friction, assuming that the stationary dislocation motion at $\tau_{ap}<\tau_p^{\rm max}$ is impossible.

However, in contrast to the constant dry friction along the glide plane, the lattice resistance stress, τ_p , is periodic along s. It is smaller than $au_p^{ ext{max}}$ almost everywhere, changes the sign, and may add to τ_{ap} along the half of the period. Besides, as long as the initial dislocation velocity and kinetic energy are high enough, for the dislocation under a shear stress of $\tau_{ap} < \tau_p + F/b$, a change of the kinetic energy $\frac{dK}{dt}$ in Eq. (1) may effectively overcome the Peierls stress. These two features allow the following phenomenon: a stationary dislocation motion at $au_{ap} \ll au_p^{ ext{max}}$. Here the stationary dislocation motion refers to a state in which the dislocation velocity is a time-independent periodic function of s with a period of b. Here the minimum au_{ap} when a stationary motion becomes possible is defined as the *dynamic Peierls stress*, τ_p^d . In a pioneering work, through including the radiation of elastic waves into the elasticity theory for dislocation motion, Al'shitz et al. [27] analytically predicted that the stationary motion of a dislocation under a fraction of the Peierls stress is possible as long as its velocity exceeds a critical value. Similarly, in an independent work with a simple atomic scale model, Crowley et al. also analytically showed that a stationary dislocation motion in materials under a shear below the static Peierls stress might happen and the external strain required for such phenomenon would strongly depend on the shape of the interatomic potential [28]. Note that the dynamic Peierls stress [27,28] was considered as a function of dislocation velocity, which is just a dissipation stress. Here we define the dynamic Peierls stress, τ_p^d , as the minimum τ_{ap} at which a stationary motion is possible. The existence of au_p^d and whether it is significantly lower than the traditional Peierls stress, τ_p^{max} , was not discussed in the literature. Later on, in a simple 2D lattice, such a phenomenon was confirmed through computer simulations at the atomic scale. The elastic wave emitted from a moving dislocation was characterized by Koizumi et al. in MD [29]. In contrast, at the continuum level, the dynamics of fast moving dislocations in materials [30] under high strain-rate deformation is usually studied through an extension of the Peierls-Nabarro model. Those models either incorporate the static Peierls stress [25,31] as one controlling parameter into the mobility law by assuming that a negligible drag has been induced by the elastic wave radiating from the moving dislocations, or simply approximate it as a viscous drag [32,33].

There obviously exists a need to perform the large-scale atomistic simulations of the motion of a dislocation below the Peierls stress in realistic materials, especially high-Peierls-barrier materials, such as silicon or other materials with covalent or ionic bonds. In particular, how far below the Peierls stress is a stationary dislocation motion possible and what are the conditions for its realization? For a continuum study of the high strain rate plastic deformation below the Peierls stress at the meso- and macro-scales, one needs a set of the constitutive equations for a single dislocation to be justified and calibrated by atomistic simulations or experiments. This will lead to an explicit incorporation of the concept of the dynamic Peierls stress, τ_p^d , into the mesoscale computer models and in turn, a significant expansion of their predictive capability.

In this paper, to confirm the existence of τ_p^d and to study the dislocation motion in a stress range of $\tau_p^d < \tau_{ap} < \tau_p$, we perform a series of MD simulations of the motion of shuffle screw and also 60° dislocations in silicon at 1 K and 300 K. Taking the dissipation force, F(v), calibrated from the MD simulations as an input, the numerical solution of Eq. (1) is also pursued. In this way, an iterative loop of linking the atomistic and continuum-level analysis is developed and closed. Surprisingly, the dynamic Peierls stresses

at 1 K is 5–7 times smaller than the static Peierls stress. We also found that the critical initial velocity $v_0^c(\tau_{ap})$ above which a dislocation can maintain a stationary motion at $\tau_p^d < \tau_{ap} < \tau_p^{\text{max}}$. After a calibration of all the material parameters in the constitutive equation (1), it well describes the MD simulation results.

2. Definition of the driving force for the motion of a dislocation

In contrast to the quasi-static processes, the definition of a driving force for the motion of a dislocation under dynamic loading is nontrivial because it is not equal to the averaged shear stress over the sample or external surface. Based on Weertman's analysis [34], the force per unit dislocation length in the direction of the Burger's vector can be calculated as follows:

$$\tau_{ap}b = \int_{-\infty}^{\infty} \tau_b(y) \frac{\partial \Delta u}{\partial y} dy. \tag{3}$$

Here τ_b is the stress distribution along the dislocation Burger's direction within the slip plane, Δu is the jump of displacements along the dislocation Burger's direction across the slip plane (see Figs. 3-5 in [26]), and the dislocation is placed at the point y=0. Since $\frac{\partial \Delta u}{\partial y}$ is not zero in the vicinity of a dislocation core only, $y \subset [-a; a]$, a small portion of the stress distribution in the interval [-a; a] will participate in the integral. Let us also assume $\frac{\partial \Delta u(-y)}{\partial y} = \frac{\partial \Delta u(y)}{\partial y}$. Then Eq. (3) can be simplified as

$$\tau_{ap}b = \int_{-a}^{0} \tau_{zx}(y) \frac{\partial \Delta u}{\partial y} dy + \int_{0}^{a} \tau_{zx}(y) \frac{\partial \Delta u}{\partial y} dy. \tag{4}$$

Utilizing the mean value theorem for the integration, we continue

$$\tau_{ap}b = \tau_b^- \int_{-a}^0 \frac{\partial \Delta u}{\partial y} dy + \tau_b^+ \int_0^a \frac{\partial \Delta u}{\partial y}$$
$$dy = (\tau_b^- + \tau_b^+) \int_0^{0.5b} d\Delta u = 0.5(\tau_b^- + \tau_b^+)b, \tag{5}$$

where τ_b^- and τ_b^+ are the averaged shear stresses in the intervals $[-a;\ 0]$ and $[0;\ a]$, respectively, and the total jump $\Delta u=b$ in the interval $[-a;\ a]$. Simulation results showed that τ_{ap} converges with an increase of a, and we choose a and τ_{ap} after a full convergence is reached. Thus,

$$\tau_{ap} = 0.5(\tau_b^- + \tau_b^+). \tag{6}$$

Since the self-stresses of a moving dislocation is antisymmetric about y=0, they do not contribute to τ_{ap} . For the static dislocation under a homogeneous external stress $\bar{\tau}$, the local stresses without considering the self-stresses are $\tau_b^-=\tau_b^+=\bar{\tau}$, and we arrive at the well-known equation. In this paper, the driving shear stress τ_{ap} for the motion of a dislocation is calculated using Eq. (6). It provides that, for constant τ_{ap} , the dislocation motion arrives at a stationary state with its velocity oscillating around a constant value, while the averaged shear stress changes.

3. Molecular dynamics simulations

Here, silicon (Si) is chosen as a representative material for verifying the possibility of a stationary dislocation motion below the static Peierls stress and the definition of a dynamic Peierls stress. The simulations are started at a low initial temperature of (1 K) using a Nosé-Hoover thermostat [35] to exclude the effect of the finite temperature on the dislocation motion. The atomic interactions are described using the Stillinger-Weber (SW) potential [36], which correctly describes the un-dissociated shuffle dislocations [12,37], the amorphous phase [38] and the GB structure in silicon [39–41]. The time step for all simulations is 1 fs. All simulations

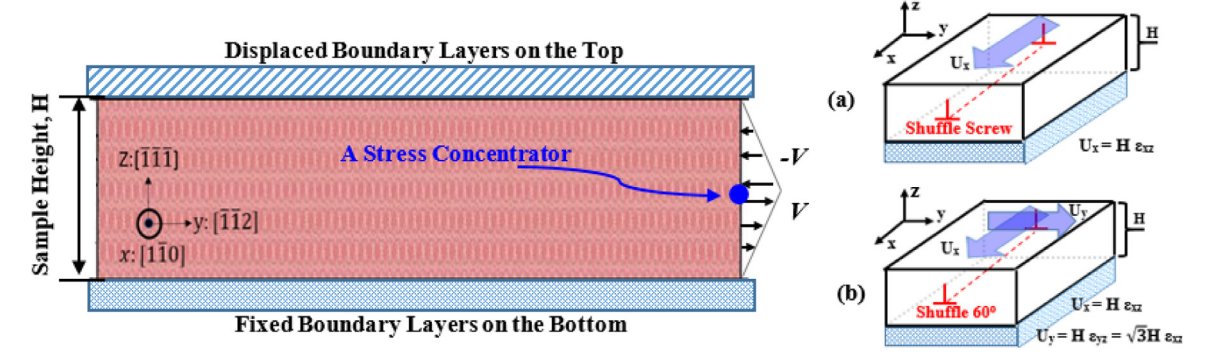


Fig. 1. The atomistic computer model set-up for simulating the single dislocation motion in single crystalline Si. The atomic displacement field corresponding to a simple shear strain ϵ_{xz} for a screw dislocation is applied in the x-y shear plane and $\epsilon_{yz}=\sqrt{3}\epsilon_{xz}$ for a shuffle 60° dislocation to produce a shear stress. The bottom of the sample is fixed as rigid and the top of it is displaced. A stress concentration is introduced on the edge of the sample when a dislocation carrying a high initial velocity needs to be generated. The inset pictures show the boundary conditions applied for a shuffle screw and 60° dislocation, respectively..

are carried out using the Large-scale Atomic/Molecular Massively Parallel Simulator (LAMMPS) [42].

Figure. 1 shows the computer model set-up of a single crystalline silicon with the xy plane parallel to the (111) glide plane. In the x-direction, a periodicity length is $L_x \approx 2\,nm$ which is larger than the cutoff distance of SW potential. The dimension of the sample along the L_x direction has been varied from $2\,nm$ to $30\,nm$. The results are found to be independent of the dimension along the sample thickness direction, where a periodic boundary condition has been applied. Along the other two dimensions, free boundary conditions are applied. L_y is the sample width along the dislocation migration direction, and has been varied from $120\,nm$ to $1000\,nm$ to exclude the size effect on the steady-state dislocation motion. L_z is fixed as a sample height of $40\,nm$. The model consists of $\approx 400,000$ to 32,000,000 atoms.

To drive the motion of a single dislocation, with a few atomic layers on the bottom of the sample being fixed, a displacement-controlled boundary condition is imposed on the top (Fig. 1). Two types of dislocations (one is shuffle 60° and the other is shuffle screw) have been considered. For the motion of a single shuffle screw dislocation, a displacement of $U_x = H\epsilon_{xz}$ along x direction is applied (Fig. 1a), where H is the height of the sample along the z direction. For the motion of the shuffle 60° dislocation, a displacement of $U_x = H\epsilon_{xz}$ together with a displacement of $U_y = H\epsilon_{yz} = \sqrt{3}H\epsilon_{xz}$ along both x and y directions are applied. For both dislocations $U_z = 0$. During the dislocation motion, the applied shear stress, τ_{ap} , is calculated using Eq. (6).

In our MD simulations, for both shuffle 60° and shuffle screw dislocations, we implement two methods to initiate dislocation motion, referred to as static loading and dynamic loading. For static loading, we drive an initially non-moving dislocation by gradually increasing the applied shear stress until it starts to move, i.e., until $\tau_{ap} > \tau_p^{\text{max}}$. A static dislocation was inserted in the middle of the sample by imposing the displacement field of dislocations [43]. After the inclusion of the dislocation, the shear strain was then increased until the dislocation start to move. The applied shear stress τ_{ap} , above which the dislocation starts to move is noted as the traditional static Peierls stress [12,43]. This method has been applied in measuring the Peierls stress for dislocations in silicon [12] and characterizing the dislocation core structure [44,45] in silicon.

For dynamic loading, we use the applied shear loading to maintain the motion of a single dislocation, which emits from a stress concentration site as shown in Fig. 1. In this dynamic loading scenario, similar to the approach in [46], the dislocation acquires a high initial velocity by introducing a strong stress concentration. Firstly, in order to nucleate the single perfect shuffle dislocation

with certain initial velocities [46-48], the constant ramped velocities along the x and y directions are imposed on the several layers of atoms located at the right boundary above and below the central glide plane in opposite directions with $V_v = \sqrt{3}V_x$ for the shuffle 60° dislocation and V_x for the shuffle screw dislocation (Fig. 1). In all simulations, $V_x = 0.001 \, nm/ps$ and the central glide plane is set between the two shuffle sets; the top right edge of the sample is displaced by 0.5b along the positive x direction and the bottom right edge by 0.5b along the negative x direction. The directions of the Burgers vector, the applied shear displacement, and the applied shear stress τ_{ap} coincide. Thereafter, the rigidly displaced atoms on the left edge of the sample remain to be fixed. Clearly, such a loading strategy is controlled by displacement rather than stress. There exists a high local stress concentration due to the velocity jump across the middle plane on the edge of sample. The maximum shear stress required by shearing a perfect crystal is at level of the theoretical yield strength and is much larger than the static Peierls stress.

In this way, the stress concentration ahead of the tip of the displacement discontinuity will produce dislocations with an initial velocity migrating towards into the simulation cell. Afterwards, the dislocation reaches a stationary velocity within 3 nm, similar to [46,49,50]. Such a loading procedure has been used for investigating supersonic dislocations in tungsten [46]. Similar stress concentrators are ubiquitous in real materials, such as steps at free surface [39,51], grain boundaries [52], interfaces between different phases [53], and the dislocation pileup against a strong obstacle or a crack [41].

4. Results and discussion

The mobility of both the initially non-moving dislocation in a static loading scenario and the dislocation carrying a high initial velocity in a dynamic loading scenario has been studied in great details here. The stationary dislocation velocity v_{st} versus the applied shear stress τ_{ap} is shown in Fig. 2. It is clear that both static and dynamic loading generate the same dislocation velocity for τ_{ap} larger than the static Peierls stress, which was determined as the applied shear stress for initiating the motion of a resting dislocation. The static Peierls stress is 1.46 GPa for shuffle 60° dislocation and 1.71 GPa for shuffle screw dislocation. Both Peierls stresses are consistent with values from the previous studies [12,22]. However, Figure. 2 also shows that the dislocation can be at a stationary motion even for τ_{ap} much lower than the static Peierls stress, if its initial velocity is high enough. Here the minimum au_{ap} that can cause the stationary dislocation motion, which we define here as the dynamic Peierls stress, τ_p^d , is 0.33 GPa for a shuffle screw dis-

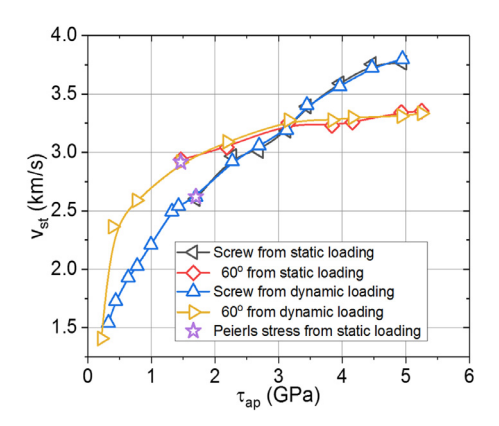


Fig. 2. The stationary dislocation velocity v_{st} versus the applied shear τ_{ap} for 60 and screw dislocations.

location and is $0.21\,GPa$ for a shuffle 60° dislocation. It should be also mentioned that the normal stress due to the fixed horizontal boundaries along the z direction in all the present simulations is much smaller than the shear stress and is thus neglected here. Also, to exclude the size effect on the dislocation motion, several simulations with $L_y\approx 1~\mu m$, the largest of which contains around 32,000,000 atoms, are carried out for $\tau_{ap}=0.4\,GPa$. Both the shuffle screw and 60° dislocations generated from the stress concentration at one end of the sample move to the other end of a sample with the same constant velocity as that observed in the small samples.

Since it is impossible with MD to determine the variation of the dislocation velocity within one Burger's vector along its glide direction, here we solve Eq. (1) to show a clear physical picture of the dynamic Peierls stress. To solve this equation, firstly, the climbing image nudged elastic band (CINEB) method [22,54-56] is used to determine the Gibbs-type energy $\bar{W}_p(\tau_{ap}, s) = W_p(\tau_{ap}, s) - \tau_{ap}bs$ under various τ_{ap} . Figure 3 shows that the energy barrier decreases with the increase of au_{ap} . In details, for a shuffle screw dislocation, the energy barrier decreases from 0.37 eV/nm at $\tau = 0$ to $0.02 \, eV/nm$ at $\tau = 1.6 \, GPa$. Through a linear extrapolation, the Peierls stress of the shuffle screw dislocation from our CINEB calculations is 1.68 GPa. Similarly, for the shuffle 60° dislocation, the energy barrier decreases from $0.29 \, eV/nm$ at $\tau = 0$ to $0.04 \, eV/nm$ at $\tau = 1.2$ GPa, and the Peierls stress is 1.39 GPa. The calculated Peierls stress corresponding to the disappearance of the barrier agrees well with that from our MD simulations.

In addition to the Peierls stress and Peierls barrier, the dissipation force F(v)/b is also calibrated through an iterative integration of Eq. (1) until its solution matches the dislocation dynamics ob-

tained in MD at $au_p^d < au_{ap} < au_{p}^{\max}$. F(v)/b is initially assumed the same as $au_{ap}(v_{st})$. Since the dislocation velocity strongly oscillates, the iteration procedure is not trivial. In previous atomistic simulations, F(v) was determined for $\tau_{ap} > \tau_p^{\text{max}}$ only; here we determine it for $\tau_{ap} \ge 0$, i.e., for a much broader range of velocities than before. Our results in Fig. 4 show that F(v) can be approximated by $F(v)/b = a e^{-cv}$, in which $a = 0.1202 \, GPa$, $c = 0.9805 \, s/km$ for the shuffle screw dislocation and $a = 1.43 \cdot 10^{-4}$ GPa, c = 3.125 s/km for the shuffle 60° dislocation. The dominant contribution to the dissipation force is believed to be induced by the phonon emission from the moving dislocations. When a dislocation moves at low speed ($v = 1.53 \, km/s$), the emitted phonon waves are confined in a cone with a wide angle of $\theta \approx 82.6^{\circ}$ behind it (Fig. 5). However, with the increase of the dislocation velocity, the phonon wave emission is largely confined within a cone with a narrow angle of $\theta \approx 54.7^{\circ}$. Note that this cone is not related to the Mach cone because the dislocation motion is still subsonic.

In the above iteration procedure, if the assumed F(v)/b leads to a higher averaged velocity, F(v)/b is then linearly increased to gradually introduce a larger drag force for dislocation motion, which in turn, will reduce the dislocation velocity. For $\tau_{ap} > \tau_p^{\rm max}$, there is no velocity oscillation, $F(v)/b = \tau_{ap}(v_{st})$, and no iterations are needed (Fig. 6). However, for $\tau_{ap} < \tau_p^{\rm max}$, there is a significant oscillation in the magnitude of the dislocation velocity. That is why F(v)/b is not equal but slightly larger than $\tau_{ap}(v_{st})$ (Fig. 6).The difference between F(v)/b and the stationary $\tau_{ap}(v_{st})$ increases with the decrease of τ_{ap} where more oscillations appear. Such differences are smaller for 60° dislocation for which F(v) and $\tau_{ap}(v_{st})$ are less sensitive to the dislocation velocity. In other words, a smaller rate-sensitivity causes smaller oscillations of the resistance stress with respect to $\tau_{ap}(v_{st})$, and, consequently, a smaller deviation of F(v) from $\tau_{ap}(v_{st})$.

Generally, the effective masses for screw and edge dislocations are adopted from [26]:

$$m = \frac{E_0}{c_t^2};\tag{7}$$

where $E_{0,i}$ is the core energy of the static dislocation and c_t is the speed of shear waves. For the SW potential we used here, $E_0 = 5.5\,eV/nm$ for the shuffle screw dislocation [57], $E_0 = 4.3\,eV/nm$ for the shuffle 60° dislocation, and $c_t = 6.4\,km/s$ [58]. Consequently, the effective mass $m_s = 1.34\dot{1}0^{-25}\,eV\cdot nm^{-3}\cdot s^{-2}$ for the shuffle screw dislocation and $m_e = 1.05*10^{-25}\,eV\cdot nm^{-3}\cdot s^{-2}$ for the shuffle 60° dislocation.

With an insertion of $\bar{W}_p(\tau_{ap},s)$, $F(\nu)$, and the effective masses of dislocations, Eq. (1) becomes

$$\frac{\partial \bar{W}_p(s, \tau_{ap})}{\partial s} + m \frac{dv}{dt} + F(v) = 0.$$
 (8)

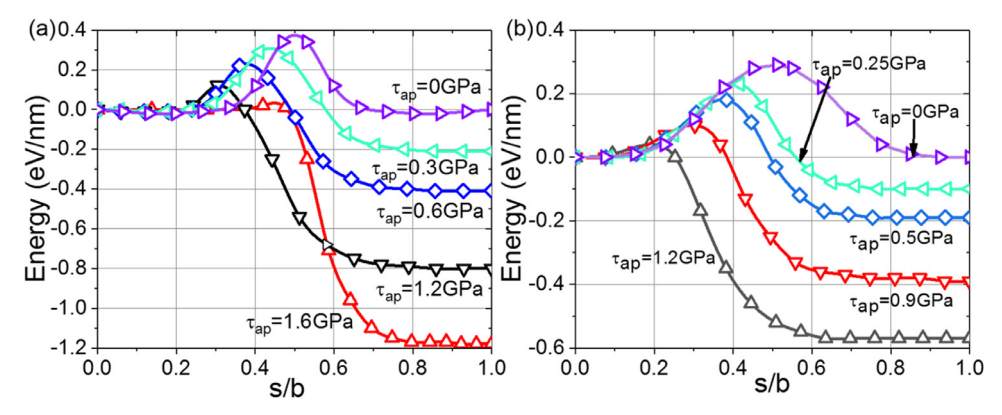


Fig. 3. The energy profile $\tilde{W}_p(\tau_{ap},s)$ and the energy barrier calculated using the CINEB method for the dislocation motion under a variety of applied shear stresses τ_{ap} along the direction of the Burgers vector.

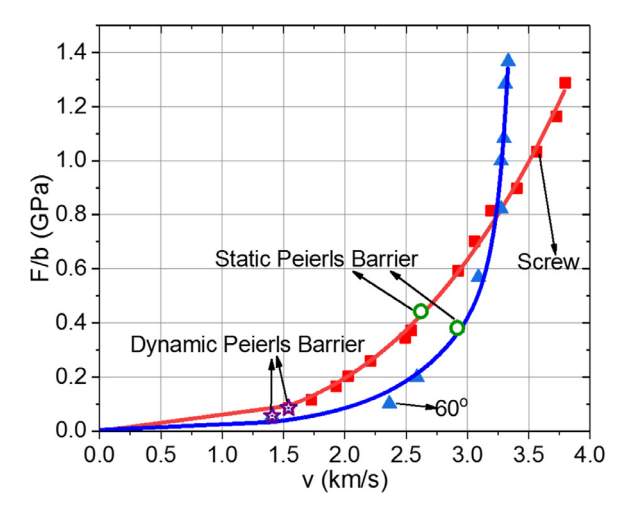


Fig. 4. The dependence of the dissipation force F/b on the dislocation velocity ν for the shuffle screw (red squares) and the 60° (blue triangles) dislocations. The two curves correspond to the analytical approximation of the atomistic data for $\tau_{ap} \geq \tau_p^d$ and a linear function for $\tau_{ap} < \tau_p^d$. (For interpretation of the references to colour in this figure legend, the reader is referred to the web version of this article.)

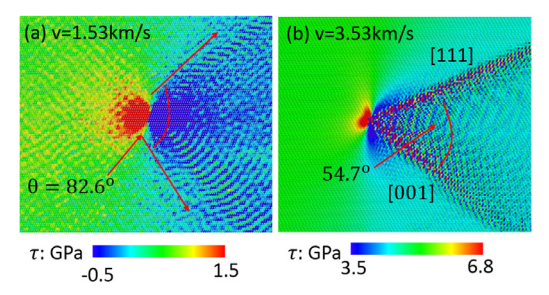


Fig. 5. The shear stress field nearby a moving dislocation at two different velocities.

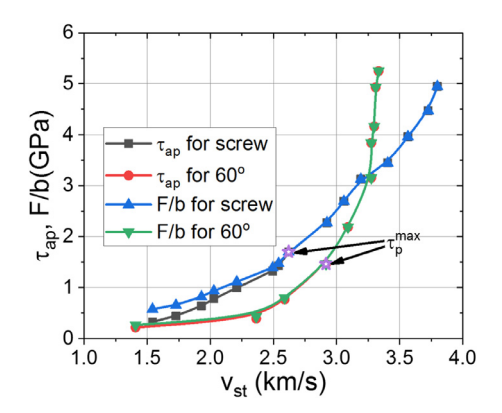


Fig. 6. A comparison of F(v)/b and $\tau_{ap}(v_{st})$.

Eq. (8) is then solved for the motion of a dislocation (initially located at s=0) with various initial velocities v_0 under different τ_{ap} . Sample solutions resulting from several different initial and boundary conditions are given in Fig. 7.

For $\tau_{ap}=0.5$ $GPa\ll \tau_p^{\rm max}$ and $v_0=3.3$ km/s the dislocation decelerates until a stationary oscillatory velocity is reached (Fig. 7 a) after moving a distance of 8b-9b. This leads to a distinctive physical picture of dislocation motion: a stationary dislocation motion at a constant averaged velocity of $v_{st}=b/t_p$, which occurs through a periodic oscillation $v_{os}(s)$ with a period of b. Here t_p is the time required for a dislocation to travel a distance of b. When the dislocation starts with an even lower initial velocity of $v_0=1.87$ km/s at $\tau_{ap}=0.7$ GPa, it accelerates to a stationary state (Fig. 7 b) at a moving distance of 6b-8b. In contrast, for $v_0=0$, dislocations can-

not move unless τ_{ap} is larger than τ_p^{max} . For $\tau_{ap}=2.2\,\text{GPa}>\tau_p^{\text{max}}$, an initially static dislocation accelerates to a constant velocity motion without oscillations through several velocity jumps (Fig. 7 c). The constant dislocation velocity corresponds to the balance between the drag and the driving force. For $\tau_{ap} = 0.1 \, GPa < \tau_n^d$, although the dislocation starts with a high velocity ($v = 4 \, km/s$), it decelerates down to zero velocity within 4-5 oscillations and then stops (Fig. 7 d). The time period for a dislocation to reach a stationary motion or a full stop is within 4-9 periods from solving Eq. (8), which is consistent with MD simulations. The good correspondences between the solution of Eq. (8) and the MD simulation results demonstrate that the calibrated $\bar{W}_p(\tau_{ap}, s)$, F(v), and the effective masses of dislocations are reasonably accurate for being used in dislocation dynamics simulations [32,33], even for $au_p^d < au_{ap} < au_p^{max}$, at which the dislocation was usually considered to be arrested.

A stationary variation of the velocity v_{st} for both types of dislocations with displacement s/b within one period of oscillation is shown in Fig. 8. The magnitude of the velocity oscillation decreases with the increase of τ_{ap} . The oscillation disappears for $\tau_{ap} > \tau_p^{\rm max}$. The minimum velocity decreases when τ_{ap} decreases. The τ_{ap} at which the minimum velocity of a shuffle screw dislocation reduces to zero is 0.36~GPa~(0.26~GPa~for~a~shuffle~60°~dislocation). This is close to the dynamic Peierls stress (0.33~GPa~and~0.21~GPa~for~shuffle~screw~and~60°~dislocations, respectively) from MD simulations.

When $\tau_p^{\max} > \tau_{ap} > \tau_p^d$, there is a critical initial dislocation velocity, $v_0^c = v_0^c(\tau_{ap})$, below which the dislocation stops (Fig. 9) and above which it continues a stationary motion, independent from how the dislocation motion was activated. The maximum v_0^c is at $\tau_{ap} = \tau_p^d$, which is $2.02 \, km/s$ for a shuffle screw dislocation and $1.89 \, km/s$ for a shuffle 60° dislocation. Then v_0^c decreases rapidly with the increase of τ_{ap} and reaches zero at $\tau_{ap} \geq \tau_p^{\max}$. The dislocation with $v_0 = 0$ at $\tau_{ap} \geq \tau_p^{\max}$ accelerates to a constant velocity as shown in Fig. 7c. The functional form of $v_0^c(\tau_{ap})$ can be approximated by $v_0^c = a(\tau_{ap} - \tau_p^{\max})^2 + b(\tau_{ap} - \tau_p^{\max})^3$ with $a = 0.2708 \, km \cdot GPa^{-2}/s$ and $b = -0.5804 \, km \cdot GPa^{-3}/s$ for a shuffle screw dislocation and $a = 1.085 \, km \cdot GPa^{-2}/s$ and $b = -0.1185 \, km \cdot GPa^{-3}/s$ for a shuffle 60° dislocation. The functional form of $v_0^c(\tau_{ap})$ can be supplemented with the dissipation force F(v) for being used in mesoscale computer simulations of plastic flow in materials under dynamic loading. For a small τ_{ap} close to τ_p^d , v_0^c increases rapidly and is significantly larger than v_{st} . However, for a large τ_{ap} , v_0^c is much smaller than v_{st} , which can still be easily reached after several periods of accelerations.

To understand whether the dislocation core structure reconstruction is responsible for or contributes to the stationary motion of a dislocation at a stress significantly below the static Peierls stress, here we exam the atomistic core structure on the fly of the dislocation motion. When the dislocation velocity is 1700 m/s and below, the core structure of the moving dislocation is found not to change in comparison with that of a static dislocation (see Fig. 10). Thus, the observed stationary dislocation motion at $\tau_{ap} \ll \tau_p^{max}$ is not caused by the core structure reconfiguration. At the same time, when au_{ap} is approaching au_p^{max} , the dislocation accelerates to a very high velocity at a level of 3000 m/s, where the core structure is found to reconstruct indeed. However, based on our results for $au_{ap} \ll au_p^{ ext{max}}$, we conclude that this is not the main reason for the stationary dislocation motion below the static Peierls stress, but just an accompanied phenomenon due to the high dislocation velocity. Additional simulations are also carried out at $T = 300 \, K$. A slight reduction in the static Peierls stress (1.65GPa and and 1.42GPa for a shuffle screw and a shuffle 60° dislocation) and a minor increase in the dynamic Peierls stress (0.45 GPa and 0.32 GPa, respectively) are observed. The increase of τ_n^d is attributed to the increase of F(v) with a temperature rise [59].

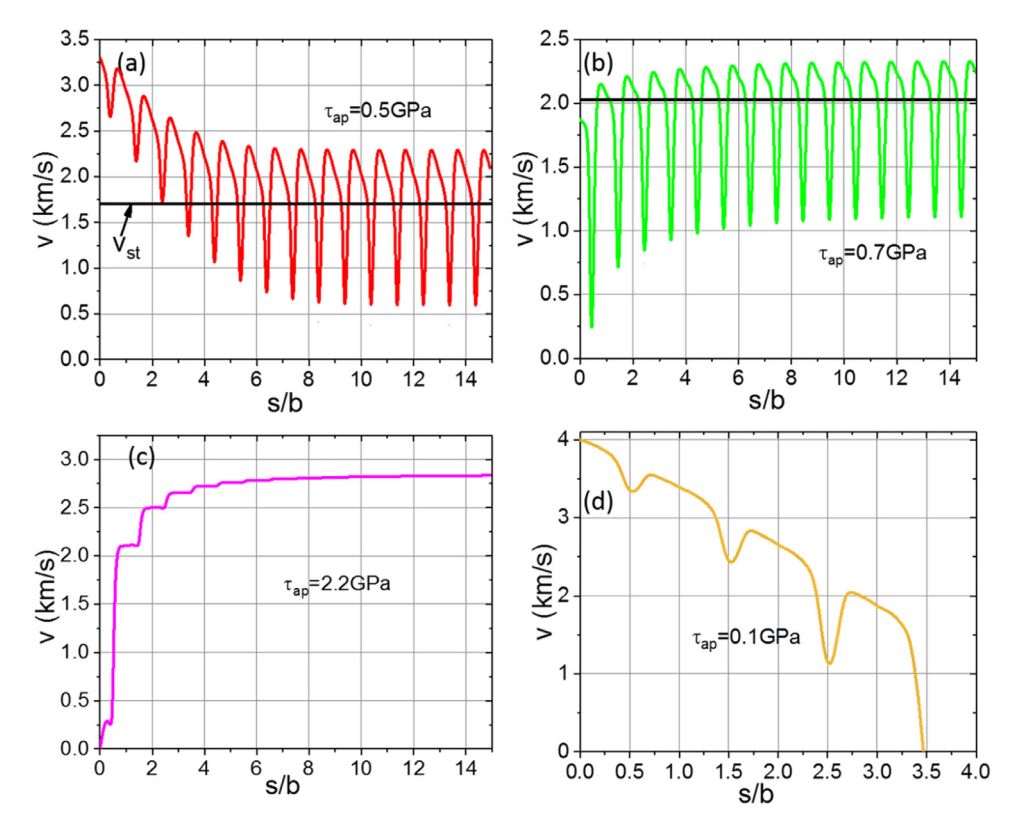


Fig. 7. The variation of a shuffle screw dislocation's velocity v as a function of its traveling distance s obtained by solving Eq. (8) using the energy profile $\tilde{W}_p(\tau_{ap},s)$ in Fig. 3 and the atomistic-data-based drag F(v) in Fig. 4 as inputs.

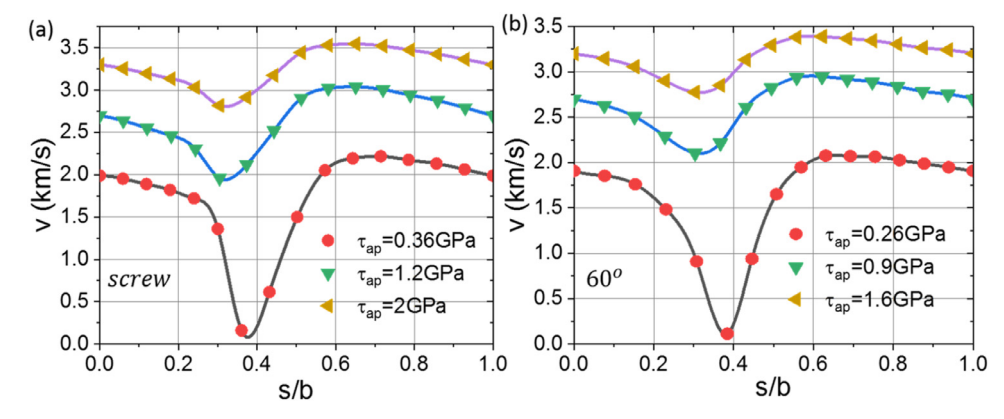


Fig. 8. A stationary variation of the velocity v of a shuffle screw dislocation (a) and 60° dislocation (b) with displacement s/b obtained by solving Eq. (8). With a decrease of τ_{ap} , the minimum velocity decreases and finally reaches zero at the dynamic Peierls stress of τ_{ap}^{b} .

The mechanisms discussed above of course do not exhaust all possible atomic modes that may contribute to the mobility of dislocations in Si. In particular, it has been widely accepted that the motion of a dislocation line in a high-Peierls-stress material like silicon do not occur by rigid translation (except in the absolute zero-temperature limit) but by thermally-induced nucleation and propagation of kinks (secondary defects along the dislocation line) at finite temperature [60-64]. The dislocation motion through a double kink mechanism is usually more energetically favorable than a rigid translation, but is ruled out here because: (i) The temperature and the applied stress in the present simulations are too low to activate a kink pair, the formation energy of which is at a level of 0.65eV and requires a stress of 1GPa at a temperature of 300K. Even under such stress and temperature conditions, according to the transient state theory, the time required to activate a kink pair will be 8 microseconds. This is obviously beyond the

reach of MD and also the main reason why the kink pairs are usually initially introduced into the computer models in many existing atomistic simulations of dislocation motion in high-Peierls-stress materials; (ii) A typical kink-kink separation along the dislocation line is at a level of 10b 12b, which is larger than the length of the dislocation line under consideration. The activities of kinks have been suppressed and are not relevant to the Peierls stress reduction observed here; (iii) The Stillinger-Weber potential has been used in this work. This interatomic potential does not produce a screw dislocation core at the center of a hexagon. Thus, with this potential, even if the kinks are initially introduced, a relaxation of the system will lead to spontaneous recombination and elimination of the kinks. However, it is also possible that the critical stress required for a stationary dislocation motion can be further reduced for some loading regimes if kinks and high initial velocity are si-

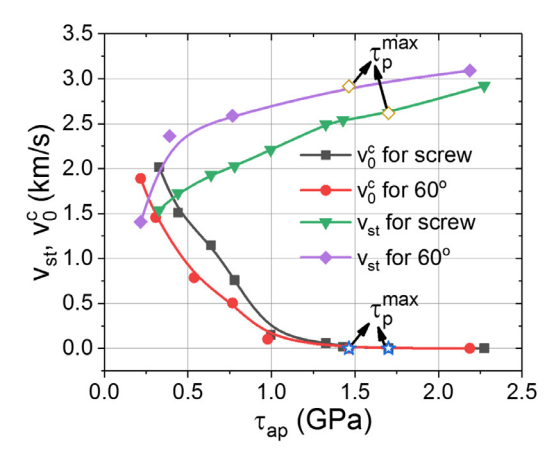


Fig. 9. The minimum initial dislocation velocity ν_0^c below which a dislocation stops vs. τ_{ap} . ν_0^c decreases from $2.02\,km/s$ for a shuffle screw dislocation and $1.89\,km/s$ for a 60° dislocation down to zero when $\tau_{ap} \geq \tau_p^{\rm max}$. For comparison, the plot of the dependence of the stationary dislocation velocity ν_{st} on τ_{ap} is also included here.

multaneously imposed on the dislocation line. This will be comprehensively studied in our future work.

In addition to assisting dislocations on overcoming the Peierls barrier, the high initial velocities and kinetic energy of dislocations may lead to other abnormal activities, which were previously observed in FCC metals only [49,50] and are reproduced here in silicon, i.e., they could be very general. For example:

- (1) A shuffle screw dislocation bounces back from the free surface when it moves at a high stationary velocity of v = 3.768 km/s(Fig. 11 b), corresponding to $\tau_{ap} > \tau_p^{\text{max}}$ (see Fig. 2 or 9). At the same time, for a low stationary velocity of v = 1.506 km/s(Fig. 11 a), which corresponds to τ_{ap} slightly larger than τ_p^d , dislocation annihilates at the surface, as expected, generating strong acoustic phonon waves. When a fast moving dislocation hits a free surface, it is also annihilated first and then a new dislocation is immediately generated, due to a high localized kinetic energy and shear stress concentration, which is four times larger than for the lower-velocity dislocation (see Fig. 11). Such an "annihilation-regeneration" process occurs in a few picoseconds and appears as if the incident dislocation has been "rebounded" from the free surface (Fig. 11b). It should be noted that such a rebounded dislocation appears on the same slip plane as that of the incident dislocation, in contrast to the similar phenomenon in metals [49,50], where it appears shifted by one slip plane. Note that the problem formulation there was the same as the above but with a longer run so that the dislocation reaches the free surface of the sample and is bounced back.
- (2) The problem formulation in Fig. 12 is the same as the above but with two dislocations nucleated from both sides of the sample. Two co-planar opposite-sign screw dislocations with

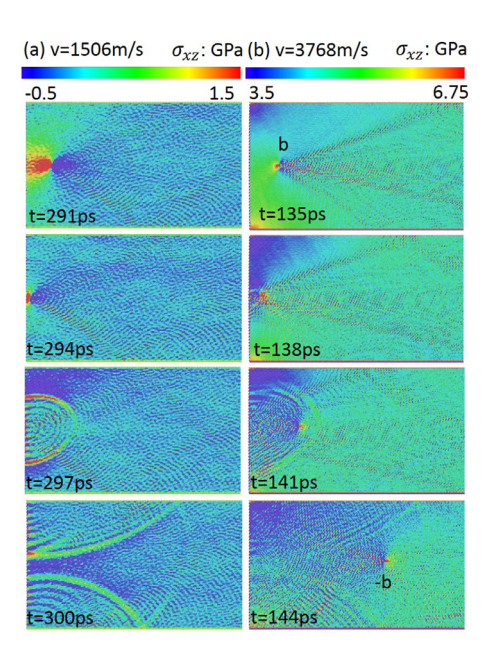


Fig. 11. (a) The annihilation of a screw dislocation on the free surface when it moves with a speed of $v=1.506\,km/s$. The kinetic energy is dissipated by the reflected acoustic phonon waves. (b) The rebounding of a screw dislocation from the free surface when it moves at a speed of $v=3.768\,km/s$. Comparing with the lowspeed dislocation in (a), the high-speed dislocation emits less intensity of phonons.

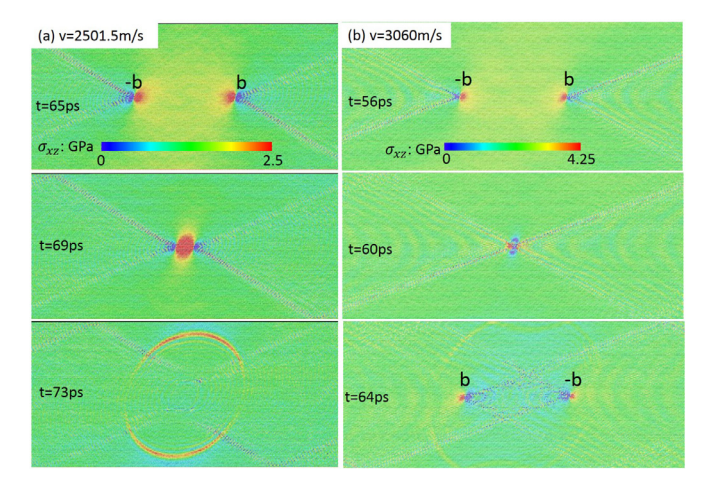


Fig. 12. (a) Two coplanar opposite-sign screw colliding dislocations annihilate when the dislocations move at v=2.501 km/s. The kinetic energy is dissipated by the acoustic phonon waves. (b) Those two same dislocations fully penetrate through each other when move against each other at v=3.06 km/s.

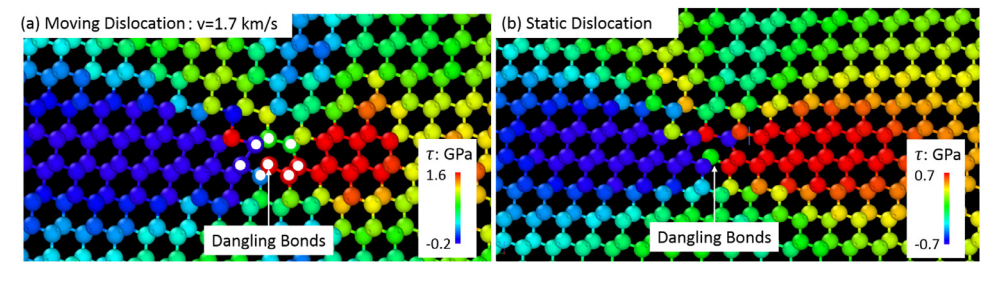


Fig. 10. A comparison of the core structures between the moving (v = 1.7 km/s) and the resting shuffle 60° dislocations. By superposing the static dislocation core structure (small white circles in (a)) on the moving dislocation core, it can be seen that motion does not change dislocation core structure. The atoms in this figure are colored by the atomic shear stresses.

high velocities of $\nu=3.060 km/s$ (corresponding to τ_{ap} slightly larger than $\tau_p^{\rm max}$) collide and penetrate each other (Fig. 12b) rather than annihilating with each other, like for $\nu=2.501 km/s$ (Fig. 12a), corresponding to $\tau_p^d < \tau_{ap} < \tau_p^{\rm max}$. When those two fast moving dislocations meet with each other on the same slip plane, they annihilate first as expected from a textbook prediction. Thereafter, driven by the high kinetic energy and the strong stress concentration, those two opposite co-planar dislocations are then immediately created and accelerated to glide in opposite directions. This process also occurs in a very short duration and looks as if the incident two dislocations have "penetrated" through each other (Fig. 12b). The acoustic wave generated by penetrated dislocations is much weaker than that by the annihilated dislocations. These phenomena will be studied quantitatively in our future research.

5. Conclusions

To summarize, we have proved and quantified the stationary motion of a dislocation in Si at $au_{ap} \ll au_p^{ ext{max}}$ using molecular dynamics simulations and solving the equation of motion for dislocations. The Peierls stress au_p^{max} is usually considered as a dry friction or a direct reflection of the yield strength. We introduced a concept of the dynamic Peierls stress $au_p^d \ll au_p^{max}$, below which a stationary dislocation motion is impossible for dislocations with any initial velocities. Starting with a qualitative analysis of the energy balance, Eq. (1), for the motion of a dislocation followed by the solutions of Eq. (8) together with MD simulations for the shuffle screw and 60° dislocations in Si at 1 K and 300 K, it is seen that, above the critical initial velocity $v_0^c(\tau_{ap})$, a dislocation can maintain a stationary motion at $\tau_p^d < \tau_{ap} < \tau_p^{\text{max}}$. The dynamic Peierls stresses at 1 K are 5–7 times smaller than the static Peierls stress. When the applied shear is between the static and dynamic Peierls barriers, if $v_0 > v_0^c(\tau_{ap})$, the dislocation velocity converges toward a stationary state at the given τ_{ap} after traveling a distance of 4b-9b, although a strong oscillation is present in the stationary velocity. Two reasons are responsible for this phenomenon:

- (a) In contrast to the constant dry friction, the lattice resistance stress, τ_p , is periodic along s, and is smaller than the Peierls stress, τ_p^{\max} , almost everywhere. It changes signs and may add to τ_{ap} along the half of the period.
- (b) When a dislocation passes the regions in which $au_{ap} < au_p + F/b$, a reduction in its kinetic energy $\frac{dK}{dt}$ in Eq. (1) acts in a way equivalent to reducing the Peierls stress.

The constitutive model for Eq. (8) includes three key components:

- (i) the energy profile $\bar{W}_p(\tau_{ap},s)$, which is calculated using the CINEB method in MD;
- (ii) the dissipation force F(v), which is determined through an iterative comparison between the solution of Eq. (8) and the MD simulation results. Previously, F(v) was determined for $\tau_{ap} \geq \tau_p^{\max}$, here F(v) is calibrated down to zero stress instead;
- (iii) and the critical initial velocity, $v_0^c(\tau_{ap})$, below which the stationary motion is not reachable.

Here Si is considered as a model material for cubic diamond and zinc blended covalent crystal structures, and the obtained results are expected to be generic for these structures. Since the energy balance equation in Eq. (1) has the same form for the partial dislocations (e.g., twinning or phase transforming dislocations) and also for twin and phase interfaces [65,66], our results here should be valid for them as well. Our findings will also open the possibility of a dynamic intensification of the plastic flow, defects accumulations, phase transformations, and shear banding [67]. Indeed,

through a dynamic initiation of dislocations and interface propagation with $\tau_{ap} > \tau_p^{\rm max}$, one can maintain a stationary dislocation at much lower stresses at $\tau_{ap} > \tau_p^d$. In particular, one possible mechanism for the drastic reduction of phase transformation pressure through plastic shearing by one to two orders of magnitude [68–70] is related to the formation of the dislocation pileups in materials. The pileup-induced strong stress concentration may activate the barrierless nucleation of a high-pressure phase [41,70–72]. The formation of such dislocation pileups can be promoted by a dynamic initiation of the plastic flow followed by a deformation at much lower stresses. Such a scenario may be realized through ball milling, short peening, or dynamic powder compaction.

Declaration of Competing Interest

The authors declare that they have no known competing financial interests or personal relationships that could have appeared to influence the work reported in this paper.

Acknowledgements

HC acknowledges supports by Shanghai Sailing Program (20YF1409400) and NSFC of China (52005186). VIL acknowledges supports of NSF (CMMI-1943710 and DMR-1904830), ONR (N00014-19-1-2082), ARO (W911NF-17-1-0225), and Iowa State University (Vance Coffman Faculty Chair Professorship). LX acknowledges the NSF support (CMMI-1930093 and DMR-1807545). VIL and LX acknowledge XSEDE computing resources under MSS170015 and MSS170003. XCZ acknowledges the support from NSFC of China (51725503).

References

- V. Bulatov, W. Cai, Computer simulations of dislocations, OSMM, OUP Oxford, 2006.
- [2] F. Roters, P. Eisenlohr, L. Hantcherli, D. Tjahjanto, T. Bieler, D. Raabe, Overview of constitutive laws, kinematics, homogenization and multiscale methods in crystal plasticity finite-element modeling: theory, experiments, applications, Acta Mater. 58 (2010) 1152–1211.
- [3] A. Arsenlis, W. Cai, M. Tang, M. Rhee, T. Oppelstrup, G. Hommes, T.G. Pierce, V.V. Bulatov, Enabling strain hardening simulations with dislocation dynamics, Model. Simul. Mater. Sci. Eng. 15 (6) (2006) 553.
- [4] C. Zhou, S.B. Biner, R. LeSar, Discrete dislocation dynamics simulations of plasticity at small scales, Acta Mater. 58 (5) (2010) 1565–1577.
- [5] W. Cai, V.V. Bulatov, Mobility laws in dislocation dynamics simulations, Mater. Sci. Eng. A 387 (2004) 277–281.
- [6] L. Pizzagalli, P. Beauchamp, First principles determination of the peierls stress of the shuffle screw dislocation in silicon, Philos. Mag. Lett. 84 (2004) 729–736.
- [7] M. Itakura, H. Kaburaki, M. Yamaguchi, First-principles study on the mobility of screw dislocations in BCC iron, Acta Mater. 60 (9) (2012) 3698–3710.
- [8] I. Shin, E. Carter, Simulations of dislocation mobility in magnesium from first principles, Int. J. Plast. 60 (2014) 58–70.
- [9] B. Yin, Z. Wu, W. Curtin, Comprehensive first-principles study of stable stacking faults in hcp metals, Acta Mater. 123 (2017) 223–234.
- [10] I. Shin, E.A. Carter, First-principles simulations of plasticity in BCC magnesium-lithium alloys, Acta Mater. 64 (2014) 198–207.
- [11] L. Pizzagalli, Stability and mobility of screw dislocations in 4H, 2H and 3C silicon carbide, Acta Mater. 78 (2014) 236–244.
- [12] C. Li, Q. Meng, G. Li, L. Yang, Atomistic simulation of the 60° dislocation mobility in silicon crystal, Superlattices Microstruct. 40 (2) (2006) 113–118.
- [13] M. Gilbert, S. Queyreau, J. Marian, Stress and temperature dependence of screw dislocation mobility in α -Fe by molecular dynamics, Phys. Rev. B 84 (17) (2011) 174103.
- [14] S. Groh, E. Marin, M. Horstemeyer, D. Bammann, Dislocation motion in magnesium: a study by molecular statics and molecular dynamics, Model. Simul. Mater. Sci. Eng. 17 (7) (2009) 075009.
- [15] C. Domain, G. Monnet, Simulation of screw dislocation motion in iron by molecular dynamics simulations, Phys. Rev. Lett. 95 (21) (2005) 215506.
- [16] N. Mathew, C. Picu, P. Chung, Peierls stress of dislocations in molecular crystal cyclotrimethylene trinitramine, J. Phys. Chem. A 117 (25) (2013) 5326–5334.
- [17] G. Monnet, D. Terentyev, Structure and mobility of the $\frac{1}{2}\langle 111\rangle \{112\}$ edge dislocation in bcc iron studied by molecular dynamics, Acta Mater. 57 (5) (2009) 1416–1426.
- [18] S. Queyreau, J. Marian, M. Gilbert, B. Wirth, Edge dislocation mobilities in bcc Fe obtained by molecular dynamics, Phys. Rev. B 84 (6) (2011) 064106.

[19] K. Edagawa, Y. Kamimura, A. Iskandarov, Y. Umeno, S. Takeuchi, Peierls stresses estimated by a discretized Peierls-Nabarro model for a variety of crystals. Materialia 5 (2019) 100218.

- [20] B. Joós, Q. Ren, M. Duesbery, Peierls-Nabarro model of dislocations in silicon with generalized stacking-fault restoring forces, Phys. Rev. B 50 (9) (1994)
- [21] G. Liu, X. Cheng, J. Wang, K. Chen, Y. Shen, Peierls stress in face-centered-cubic metals predicted from an improved semi-discrete variation Peierls-Nabarro model, Scr. Mater. 120 (2016) 94-97.
- [22] Z. Li, N. Mathew, R. Picu, Dependence of Peierls stress on lattice strains in silicon, Comput. Mater. Sci. 77 (2013) 343–347.
- [23] D. Ferré, P. Carrez, P. Cordier, Modeling dislocation cores in SrTiO₃ using the Peierls-Nabarro model, Phys. Rev. B 77 (1) (2008) 014106.
- [24] Y. Xiang, H. Wei, P. Ming, W. E, A generalized Peierls-Nabarro model for curved dislocations and core structures of dislocation loops in al and cu, Acta Mater. 56 (7) (2008) 1447-1460.
- [25] G. Po, Y. Cui, D. Rivera, D. Cereceda, T. Swinburne, J. Marian, N. Ghoniem, A phenomenological dislocation mobility law for bcc metals, Acta Mater. 119 $(2016)\ 123-135.$
- [26] J.P. Hirth, J. Lothe, Theory of dislocations, Krieger Publishing Company, 1992.
- [27] V. Al'shitz, V. Indenbom, A. Shtol'berg, The peierls dynamic force, Zh. Eksp. Teor. Fiz 60 (1971) 2308–2320. [28] S. Crowley, N. Flytzanis, V. Celli, Dynamic peierls stress in a crystal model with
- slip anisotropy, J. Phys. Chem. Solids 39 (10) (1978) 1083-1088.
- [29] H. Koizumi, H. Kirchner, T. Suzuki, Lattice wave emission from a moving dislocation, Phys. Rev. B 65 (21) (2002) 214104.
- [30] L. Pillon, C. Denoual, Y. Pellegrini, Equation of motion for dislocations with inertial effects, Phys. Rev. B 76 (22) (2007) 224105.
- [31] Z. Wang, I. Beyerlein, An atomistically-informed dislocation dynamics model for the plastic anisotropy and tension-compression asymmetry of bcc metals, Int. J. Plast. 27 (10) (2011) 1471–1484. Conventional and Emerging Materials
- [32] M. Shehadeh, H. Zbib, On the homogeneous nucleation and propagation of dislocations under shock compression, Philos. Mag. 96 (26) (2016) 2752-2778.
- [33] J. Hu, Z. Liu, K. Chen, Z. Zhuang, Investigations of shock-induced deformation and dislocation mechanism by a multiscale discrete dislocation plasticity model, Comput. Mater. Sci 131 (2017) 78-85.
- [34] J. Weertman, J. Weertman, Moving dislocations, in: F. Nabarro (Ed.), Dislocations in Solids, 3, 1980.
- [35] D. Evans, B. Holian, The nose-hoover thermostat, J. Chem. Phys. 83 (8) (1985) 4069-4074.
- [36] F. Stillinger, T. Weber, Computer simulation of local order in condensed phases of silicon, Phys. Rev. B 31 (8) (1985) 5262.
- [37] W. Cai, V. Bulatov, J. Chang, J. Li, S. Yip, Anisotropic elastic interactions of a periodic dislocation array, Phys. Rev. Lett. 86 (25) (2001) 5727
- [38] Sastry S., Angell C., Liquid-liquid phase transition in supercooled silicon, Nat. Mater. 11 739.
- [39] X. Chen, L. Xiong, A. Chernatynskiy, Y. Chen, A molecular dynamics study of tilt grain boundary resistance to slip and heat transfer in nanocrystalline silicon, J. Appl. Phys. 116 (24) (2014) 244309.
- [40] H. Chen, V. Levitas, L. Xiong, Slip of shuffle screw dislocations through tilt grain boundaries in silicon, Comput. Mater. Sci. 157 (2019) 132-135.
- [41] H. Chen, V. Levitas, L. Xiong, Amorphization induced by 60° shuffle dislocation pileup against different grain boundaries in silicon bicrystal under shear, Acta Mater. 179 (2019) 287-295.
- [42] S. Plimpton, Fast parallel algorithms for short-range molecular dynamics, J. Comput. Phys. 117 (1) (1995) 1–19.
- [43] D. Hull, D. Bacon, Introduction to dislocations, Butterworth-Heinemann, 2001.
- [44] W. Cai, V. Bulatov, J. Chang, J. Li, S. Yip, Periodic image effects in dislocation modelling, Philos. Mag. 83 (5) (2003) 539-567.
- [45] W. Cai, V. Bulatov, J. Chang, J. Li, S. Yip, Dislocation core effects on mobility, Dislocations in solids 12 (2004) 1-80.
- [46] P. Gumbsch, H. Gao, Dislocations faster than the speed of sound, Science 283 (5404) (1999) 965-968.
- [47] Z. Jin, P. Gumbsch, E. Ma, K. Albe, K. Lu, H. Hahn, H. Gleiter, The interaction mechanism of screw dislocations with coherent twin boundaries in different face-centred cubic metals, Scr. Mater. 54 (6) (2006) 1163-1168.

[48] Z. Jin, P. Gumbsch, K. Albe, E. Ma, K. Lu, H. Gleiter, H. Hahn, Interactions between non-screw lattice dislocations and coherent twin boundaries in facecentered cubic metals, Acta Mater. 56 (5) (2008) 1126-1135.

- [49] Q. Li, J. Li, Z. Shan, E. Ma, Strongly correlated breeding of high-speed dislocations, Acta Mater. 119 (2016) 229-241.
- [50] O. Li, J. Li, Z. Shan, E. Ma, Surface rebound of relativistic dislocations directly and efficiently initiates deformation twinning, Phys. Rev. Lett. 117 (16) (2016) 165501.
- [51] A. Latapie, D. Farkas, Molecular dynamics simulations of stress-induced phase transformations and grain nucleation at crack tips in fe, Modell. Simul. Mater. Sci. Eng. 11 (5) (2003) 745.
- E. Gulervuz, S. Mesarovic, Dislocation nucleation on grain boundaries; low angle twist and asymmetric tilt boundaries, Crystals 6 (7) (2016) 77.
- I. Salehinia, J. Wang, D. Bahr, H. Zbib, Molecular dynamics simulations of plastic deformation in nb/nbc multilayers, Int. J. Plast. 59 (2014) 119–132. [54] R. Gröger, V. Vitek, Stress dependence of the Peierls barrier of $\frac{1}{2} < 111 >$ screw
- dislocations in bcc metals, Acta Mater. 61 (17) (2013) 6362-6371.
- [55] G. Henkelman, H. Jónsson, Improved tangent estimate in the nudged elastic band method for finding minimum energy paths and saddle points, J. Chem. Phys. 113 (22) (2000) 9978-9985.
- G. Henkelman, B. Uberuaga, H. Jónsson, A climbing image nudged elastic band method for finding saddle points and minimum energy paths, J. Chem. Phys. 113 (22) (2000) 9901–9904.
- [57] L. Pizzagalli, P. Beauchamp, J. Rabier, Undissociated screw dislocations in silicon: calculations of core structure and energy, Philos. Mag. 83 (10) (2003) 1191-1204.
- [58] E. Hahn, S. Zhao, E. Bringa, M. Meyers, Supersonic dislocation bursts in silicon, Sci. Rep. 6 (2016) 26977.
- [59] E. Bitzek, P. Gumbsch, Dynamic aspects of dislocation motion: atomistic simulations, Mater. Sci. Eng. A 400 (2005) 40-44.
- [60] L. Pizzagalli, P. Beauchamp, Dislocation motion in silicon: the shuffle-glide controversy revisited, Philos. Mag. Lett. 88 (6) (2008) 421-427.
- [61] A. Pedersen, L. Pizzagalli, H. Jonsson, Finding mechanism of transitions in complex systems: formation and migration of dislocation kinks in a silicon crystal, Phys.: Condens. Matter 21 (2009) 084210.
- [62] S. Wang, L. Huang, R. Wang, The 90° partial dislocation in semiconductor silicon: an investigation from the lattice p-n theory and the first principle calculation, Acta Mater. 109 (2016) 187-201.
- [63] L. Huang, S. Wang, Structure and energy of the (110) screw dislocation in silicon using generalized peierls theory, J. Appl. Phys. 125 (2019) 145702.
- [64] R. Ji, T. Phan, H. Chen, L. Xiong, Quantifying the dynamics of dislocation kinks in iron and tungsten through atomistic simulations, Int. J. Plast. 128 (2020) 102675.
- [65] G. Olson, M. Cohen, Dislocation theory of martensitic transformations, in: F. Nabarro (Ed.), Dislocations in Solids, 7, 1986, p. 297.
- [66] M. Grujicic, G. Olson, Dynamics of martensitic interfaces, Interface Sci. 6 (1-2) (1998) 155-164.
- [67] T. Phan, R. Ji, Y. Chen, A. Bastawros, L. Xiong, Metallic glass instability induced by the continuous dislocation absorption at an amorphous/crystalline interface, Acta Mater. (2020).
- [68] C. Ji, V. Levitas, H. Zhu, J. Chaudhuri, A. Marathe, Y. Ma, Shear-induced phase transition of nanocrystalline hexagonal boron nitride to wurtzitic structure at room temperature and lower pressure, Proc. Natl. Acad. Sci. 109 (47) (2012) 19108-19112.
- [69] Y. Gao, Y. Ma, Q. An, V. Levitas, Y. Zhang, B. Feng, J. Chaudhuri, W. Goddard III, Shear driven formation of nano-diamonds at sub-gigapascals and 300 k, Carbon 146 (2019) 364-368.
- V. Levitas, High-pressure phase transformations under severe plastic deformation by torsion in rotational anvils, Mater. Trans. 60 (7) (2019) 1294–1301. [71] M. Javanbakht, V. Levitas, Phase field simulations of plastic strain-induced
- phase transformations under high pressure and large shear, Phys. Rev. B 94 (21) (2016) 214104.
- V. Levitas, S. Esfahani, I. Ghamarian, Scale-free modeling of coupled evolution of discrete dislocation bands and multivariant martensitic microstructure, Phy. Rev. Lett. 121 (20) (2018) 205701.